Available online at www.sciencedirect.com
SCIENCE DIRECT®
C. R. Chimie 8 (2005) 753–763
COMPTES RENDUS CHIMIE
http://france.elsevier.com/direct/CRAS2C/

Full paper / Mémoire

Metal organic frameworks based on Cu^{2+} and benzene-1,3,5-tricarboxylate as host for SO_2 trapping agents

Hendrik Dathe, Elvira Peringer, Virginia Roberts, Andreas Jentys, Johannes A. Lercher *

Department of Chemistry, Technische Universität München, Lichtenbergstraße 4, 85747 Garching, Germany

Received 30 July 2004; accepted 21 October 2004

Available online 12 February 2005

Abstract

Metal organic framework materials with Cu^{2+} as central cation and benzene-1,3,5-tricarboxylate (BTC) as linker were prepared via hydrothermal synthesis and impregnated with barium salts (chloride, nitrate, acetate) to explore the role of the Ba^{2+} counter ion on the SO_2 uptake. The impregnation of the metal organic framework materials with barium salts led to a decrease of pore volume through the (intra pore) formation of small Ba salt crystals. The structure of the Cu–BTC material was preserved after the impregnation with acetate and nitrate, but partially destroyed during impregnation with chloride. The complete loss of the BTC structure occurred through thermal decomposition at temperatures around 573 K. The sample impregnated with $BaCl_2$ showed a higher fraction of Cu^{2+} species compared to the other Ba/Cu–BTC samples. The SO_2 uptake capacity of the Ba/Cu–BTC(Cl^-) sample was the highest at temperatures below 673 K among all materials prepared and even higher compared to $BaCO_3/Al_2O_3$/Pt based material. The comparison of the theoretical uptake (based on the stoichiometric formation of $BaSO_4$) with the maximum SO_x uptake achieved on the Ba/Cu–BTC samples clearly points out that a fraction of the SO_x is stored on the Cu species being part of the metal organic framework structure. With increasing temperature the framework is (partially) decomposed and highly dispersed Cu species are released, which act as additional SO_x storage sites in the high temperature region. ***To cite this article: H. Dathe et al., C. R. Chimie 8 (2005).***

Résumé

Des composés organométalliques, avec Cu^{2+} comme cation central et le 1,3,5-tricarboxylatebenzène (BTC) comme ligand, ont été préparés par synthèse hydrothermique et imprégnés par des sels de barium (chlorate, nitrate, acétate) pour permettre l'étude du rôle du contre-ion Ba^{2+} dans l'absorption du SO_2. L'imprégnation des structures organométalliques avec les sels de barium a mené à la diminution du volume des pores, du fait de la formation (à l'intérieur des pores) de petits cristaux de sels de baryum. La structure du Ca–BTC a été préservée après l'imprégnation avec l'acétate et le nitrate, mais, d'un autre côté, elle a été partiellement détruite durant l'imprégnation avec le chlorate. La perte totale de la structure du BTC survient lors d'une décomposition thermique à une température voisine de 573 K. L'échantillon imprégné avec le $BaCl_2$ possède une plus grande propor-

* Corresponding author.
E-mail address: Johannes.lercher@ch.tum.de (J.A. Lercher).

1631-0748/$ - see front matter © 2005 Académie des sciences. Published by Elsevier SAS. All rights reserved.
doi:10.1016/j.crci.2004.10.018

tion d'ions Cu^{2+} comparé à l'autre l'échantillon (Ba/Cu–BTC). La plus haute capacité d'absorption de SO_2 par les échantillons de Ba/Cu–BTC a été observée à des températures au-dessous de 673 K pour tous les matériaux préparés, et une capacité supérieure a même été observée en comparaison des matériaux industriels. La comparaison entre les valeurs théoriques d'absorption (fondées sur la formation stœchiométrique du $BaSO_4$) et la valeur maximale d'absorption des SO_x, obtenue avec les échantillons de Ba/Cu–BTC, nous démontre clairement qu'une fraction de SO_x est emmagasinée sur le Cu de la structure organométallique. Avec l'augmentation de la température, la structure est partiellement décomposée et les ions Cu hautement dispersés sont libérés, ce qui a pour effet de créer des sites d'emmagasinement supplémentaires. ***Pour citer cet article : H. Dathe et al., C. R. Chimie 8 (2005).***

Keywords: Metal organic frameworks; XANES; SO_2 trapping; Copper complexation

Mots clés : Structures organométallique ; XANES ; Piégeage du SO_2 ; Complexation du cuivre

1. Introduction

Three-dimensionally linked metal organic frameworks [1–6] can lead to void structures capable of sorbing organic and inorganic molecules. Unlike oxide based microporous molecular sieves the reticulated structure of the metal organic frameworks is established by linking metal cations or clusters with bi- or multi-dentate organic ligands. Recently substantial progress has been made with respect to the rational synthesis of such materials and a large number of metal organic frameworks have been made with tailored micro- and mesoporosity [7–11]. Typically metal cations of Zn, Cu, Co, Ru, Os and rare earth metals are used [12] in combination with O-bridging linkers, e.g. benzene-1,3,5-tricarboxylate (BTC), N-bridging linkers, e.g. 4,4′-bipyridine or S-bridging linkers, e.g. biphenyldisulfonic acid.

The dimensionality of the Me–BTC frameworks mainly depends on the solvent used for the synthesis and the strength of base employed for the H_3BTC deprotonation. With a strong conjugate base (e.g. the acetate anion acting as a strong coordinating ligand) and water as solvent (and strong coordinating ligand) a porous one-dimensional framework will be obtained. Using a less strongly coordinating solvent such as ethanol and a weaker base such as pyridine for deprotonation a porous two-dimensional structure will be obtained. Pyridine partly deprotonates H_3BTC and, in the absence of water, binds strongly to metal ions blocking so the extension of the framework. For three-dimensional structures a stronger base, such as triethylamine, with sufficient strength to completely deprotonate H_3BTC, but with a low affinity for binding to metal ions is necessary [13].

The rigid and divergent character of the linker added, e.g. carboxylates, leads to high pore volumes (up to 91.1% of the crystal volume) and in consequence high apparent surface areas of up to 2500 m^2/g for three-dimensional structures [14,15]. The coordination chemistry allows locking the metal ions in their positions within the M–O–C clusters, referred to as secondary building units (SBUs). The SBUs serve as large rigid vertices that can be joined by rigid organic links to produce neutral charged extended frameworks without counter ions in their cavities.

MOF materials typically lose their integrity and structure above 573 K. The control of the architecture by variation of the organic linkers and the functionalization of the pores with organic groups, like –Br, $–NH_2$, $–OC_3H_7$, $–OC_5H_{11}$, $–C_2H_4$, $–C_4H_4$ [3,9] allows a flexible design of these materials. After removal of the solvent molecules, which act as a ligand a high concentration of coordinative unsaturated coordination sites on the metal ions, accessible from all direction from the three-dimensional channels are produced.

As an example for MOF materials, the structure of copper(II) benzene-1,3,5-tricarboxylate – $[Cu_3(BTC)_2(H_2O)_3]_n$ – (denoted as Cu–BTC) will be discussed. Cu–BTC is a neutral coordination polymer composed of dimeric cupric tetracarboxylate units [8]. Twelve carboxylate oxygen atoms from two BTC ligands, which bind to the four coordination sites of the three Cu^{2+} ions present in the SBU. These copper–benzenecarboxylate units form a face-centered crystal lattice of *Fm*3*m* symmetry, which has a complex three-dimensional channel system. Terminal water ligands,

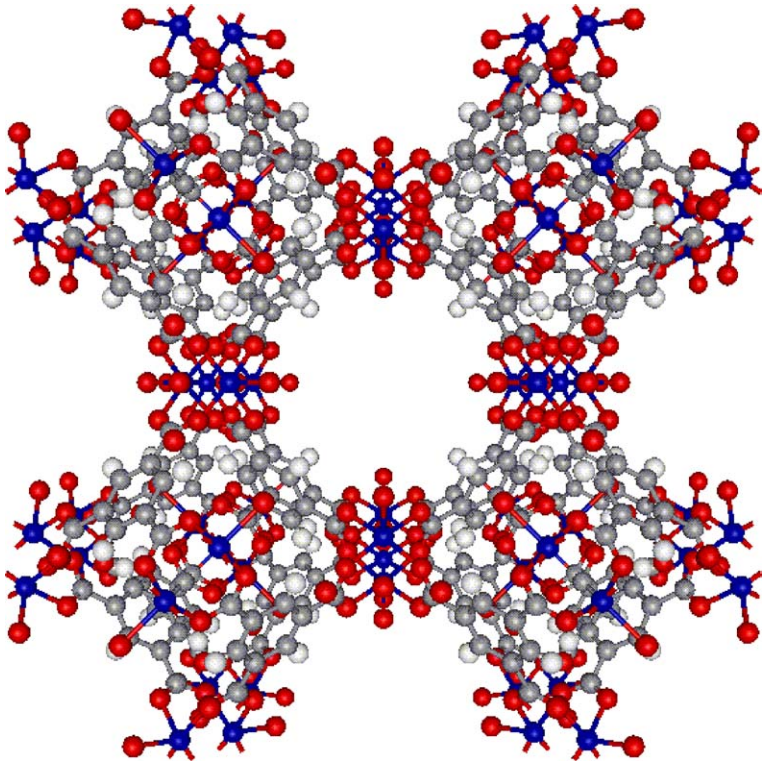

Fig. 1. Crystal structure of the Cu–BTC.

bound to the copper ions, are directed towards the interior of these pore system. A crystal structure of the material is shown in Fig. 1. The main pores of approximately 0.9 nm diameter form a cubic network with additional side pockets formed by planar $C_6H_3(O_2C)_3$ segments. These tetrahedron-shaped windows of these pockets have a diameter of about 0.35 nm. This is wide enough for a penetration of small gas molecules in the network while larger organic molecules are excluded [12]. Promising applications of MOF materials include gas sorption, e.g. hydrogen storage [9,11,13], gas separation and catalysis [16,17].

The ultra-large pore volume makes these materials ideal candidates for supporting a second phase inside the pores, which allows creating multifunctional materials with keeping an appreciable reaction volume. In the work presented we focus on describing the synthesis, characterization and testing of novel sulfur trap materials, to be potentially used as guards for NO_x storage reduction catalysts to prevent admission of SO_x, which leads to a rapid decrease of the storage capacity by forming highly stable sulfates [18,19]. In such 'sulfur traps', SO_2 formed from the combustion of S impurities present in the fuel needs to be oxidized to SO_3 first, which in turn will be chemisorbed as sulfate by alkaline earth cations such as Ba^{2+}. In conventional oxide based materials supported barium oxide or carbonate will act as trapping agent, while Pt is added as oxidation catalyst. The materials discussed here will be based on Cu^{2+} (probably on defect sites) acting as oxidizing component, while supported barium salts will be providing sites for SO_3 chemisorption.

2. Experimental

2.1. Synthesis of materials

The synthesis method used was adapted from the synthesis route described by Vishnyakov et al. [12]. Benzene-1,3,5-tricarboxylic acid (12.28 g, 0.059 mol, Merck) was dissolved in 62.5 ml ethanol (Merck) and cupric nitrate hydrate $Cu(NO_3)_2 \cdot 3\ H_2O$ (28.15 g, 0.117 mol, Merck) was dissolved in 62.5 ml water. The two solutions were mixed at ambient temperature for 30 min and subsequently transferred into a 120 cm^3

PTFE-lined stainless steel autoclave, which was heated to 383 K under hydrothermal conditions for 18 h. The reaction vessel was cooled to ambient temperature and the blue crystals of Cu–BTC were isolated by filtration and washed with water. The solid product was dried overnight at 383 K. The yield achieved was nearly 100% (18.13 g Cu–BTC).

For the impregnation, $BaCl_2 \cdot 2\,H_2O$ (0.81 g, 0.003 mol, Merck), $Ba(CH_3COO)_2$ (0.76 g, 0.003 mol) or $Ba(NO_3)_2$ (0.78 g, 0.003 mol) was dissolved in 60 ml alcohol/water mixture (1:1) and 2 g of Cu–BTC (dried at 435 K for 4 h) was added to the solution. The mixture was stirred for 22.5 h at ambient temperature. The solvent was removed under reduced pressure and the blue material was finally dried at 383 K. For comparison a model catalyst containing (2%) Pt (oxidation/reduction components), (10%) $BaO/BaCO_3$ (SO_x storage component) on an Al_2O_3 support was used.

2.2. Characterization

The crystalline structure of the synthesized and modified materials was analyzed by XRD using a *Philips X'Pert Pro System* (Cu Kα1-radiation, 0.154056 nm) operating at 40 kV/40 mA. Measurements were performed in a glass capillary ($\phi = 0.5$ mm) with a scan step of 0.05°/min from 5° to 80° 2θ. The morphology and particle size of the synthesized materials were examined by scanning electron microscopy using a *JEOL* 500 SEM-microscope (accelerating voltage 23 kV). For SEM experiments the samples were outgassed for 2 days and sputtered with gold before collecting the images. Nitrogen adsorption measurements were collected at 77.4 K with a PMI automated BET Sorptometer. For BET measurements the samples were outgassed at 473 K in vacuum (10^{-3} Pa) for 24 h prior to the adsorption measurements. The mesopore size distribution was obtained from the desorption branch of the isotherm using the Barret–Joyner–Halenda (BJH) method, the micropore volume was obtained from the desorption branch of the isotherm using Horvath–Kawazoe (HK) method.

The thermal stability of the materials was investigated by thermogravimetric methods in a modified *Setaram TG-DSC 111* system. The samples were pressed into thin wafers and subsequently broken into small platelets. Approximately 18 mg of these platelets were charged into the quartz samples holder of the balance. The samples were heated in vacuum with a temperature increment of 10 K/min to 973 K. Changes in weight were observed and the gases evolved were analyzed with a Balzers quadrupole mass spectrometer.

The chemical composition of materials synthesized was determined by atomic absorption spectroscopy (AAS) using a *UNICAM 939 AA-Spectrometer*.

For X-ray absorption spectroscopy the samples were pressed into self supported wafers with a total absorption 2.5. X-ray absorption spectra were measured at HASYLAB, DESY (Hamburg, Germany) on beam line X1 and E4 using a Si (111) monochromator. The contributions of higher order reflections were excluded by detuning the second crystal of the monochromator to 60% of the maximum intensity. The spectrum of the corresponding metal foil was recorded simultaneously between the second and a third ionization chamber to calibrate the energy alignment of the monochromator. X-ray absorption spectra were recorded at the Cu–K edge at liquid nitrogen temperature. For the analysis of the EXAFS the oscillations were extracted from the background using a combination of a first and third order polynomial function and after weighting with k^2 the oscillations were Fourier transformed in the range between 2.1 and 15 per Å. The local environment of the Cu atoms was determined from the analysis of the EXAFS in k-space using phase-shift and amplitude functions for Cu–O and Cu–Cu calculated assuming multiple scattering processes (FEFF Version 8.10) using the program Viper to analyze the data [20,21].

2.3. SO_x uptake

The SO_x uptake rate was determined in a plug flow reactor system equipped with a fluorescence detector (Model 43C *Fa.* Thermo Environmental Instruments) to monitor the SO_2 concentration at the reactor outlet. As the detector can only monitor the SO_2 concentration in the gas stream a converter operating at 1223 K was placed behind the reactor to convert SO_3 formed during the reaction to SO_2. For distinction between SO_2 and SO_3 experiments with and without converter were carried out. For the SO_2 uptake experiments 50 mg of the storage material (particle size 0.3–0.6 mm) was diluted with 100 mg SiC (particle size < 0.3 mm) and exposed to a flow of 50 ppm SO_2 and 6% O_2 in He at a flow rate of 200 ml/min. After heating up to 473 K with 10 K/min the SO_x breakthrough over the catalyst bed was followed at 473, 573, 673 and 773 K.

3. Results and discussion

3.1. Composition, morphology and porosity of the materials

The compositions and N_2 physisorption results of the parent Cu–BTC and of the Ba^{2+} loaded materials are shown in Table 1. Due to the lower solubility of Ba-nitrate in the water/ethanol mixture the Ba^{2+} concentration for the Ba/Cu–BTC(NO_3^-) sample was 7.5 wt.%, while for the other Ba^{2+} containing samples a loading of 15 wt.% Ba was reached. The N_2 adsorption/desorption isotherms of Cu–BTC and Ba/Cu–BTC are compared in Fig. 2. The isotherms of Cu–BTC correspond to a type I isotherm, typical for micropouros materials, whereas the impregnated samples show a type IV isotherm typical for materials with mesopores. The highest pore volume was observed for the parent Cu–BTC, while after impregnation with the Ba salts the pore volume decreased. A comparison of the pore volumes analyzed with the different methods showed that it strongly decreased (especially the volume of the micropores) after impregnation with Ba-chloride.

The XRD patterns of the Ba^{2+} impregnated Cu–BTC samples are compiled in Fig. 3. The XRD of the parent Cu–BTC was in perfect agreement with the X-ray diffractogram simulated using the program MERCURY and the crystal structure reported in Ref. [8]. After impregnation with Ba-acetate and Ba-nitrate strong reflections around $2\theta = 25°$ and 38° were observed, which are assigned to acetate and nitrate species. In contrast for Cu–BTC impregnated with $BaCl_2$ the intensity of all XRD reflections decreased indicating a decrease in crystallinity. The basic patterns of the Cu–BTC structure observed for the samples impregnated with nitrate and acetate indicate that the metal organic framework structure was preserved, while for the $BaCl_2$ impregnated sample the smaller reflections indicate a significant reduction of the coherence in the metal organic framework structure.

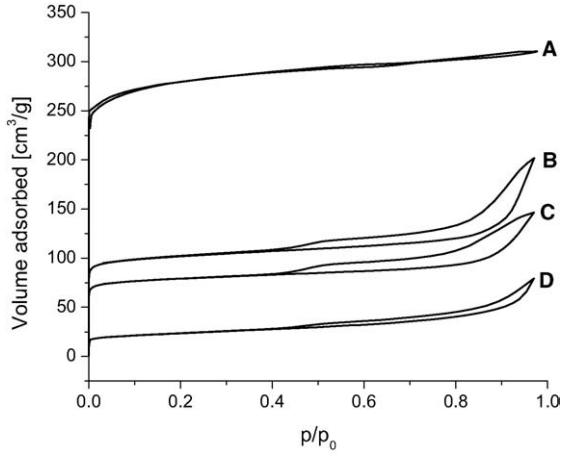

Fig. 2. N_2 adsorption/desorption isotherms of the prepared MOF samples. ((A) Cu–BTC (B) Ba/Cu–BTC(CH_3COO^-) (C) Ba/Cu–BTC(NO_3^-) (D) Ba/Cu–BTC(Cl^-)).

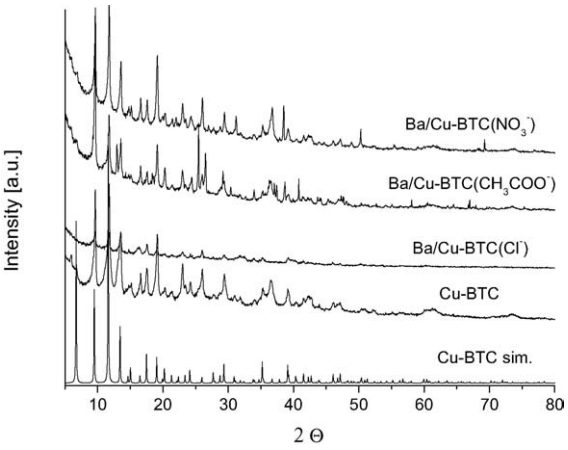

Fig. 3. XRD patterns of Cu–BTC and Ba/Cu–BTC samples.

Scanning electron microscopy images from Cu–BTC and $BaCl_2$ impregnated Cu–BTC are compared in Figs. 4 and 5, respectively. Cu–BTC crystallized in double sided pyramids with an edge length in the range of 130–215 μm and a height of 170–230 μm. Besides these large crystals, also smaller crystals with an edge length around 15 μm and height of 20 μm were formed.

Table 1
AAS and N_2 physisorption results of synthesized MOF samples

Sample	Ba (wt.%)	Cu (wt.%)	Pore volume >16 Å (BJH) (cm^3/g)	Pore volume 4–20 Å (HK) (cm^3/g)
Cu–BTC	–	26.2	0.1359	0.417761
Ba/Cu–BTC(CH_3COO^-)	15.2	22.5	0.1398	0.120883
Ba/Cu–BTC(NO_3^-)	7.5	27.2	0.1997	0.155452
Ba/Cu–BTC(Cl^-)	14.9	26.3	0.1157	0.035272

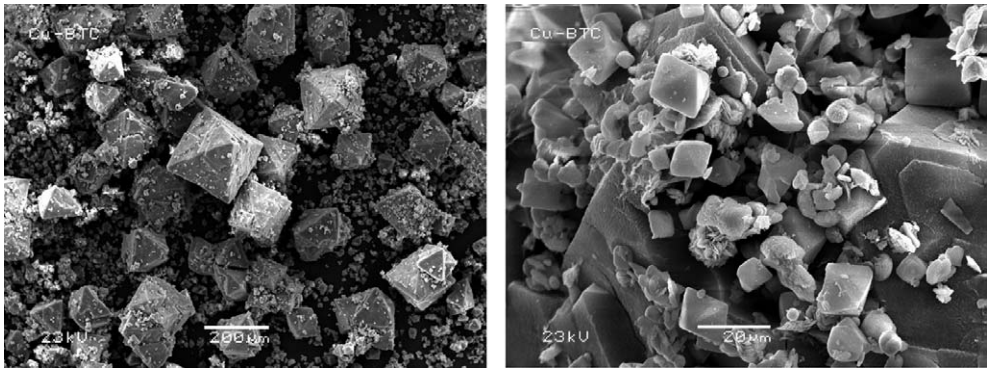

Fig. 4. Scanning electron micrographs of Cu–BTC.

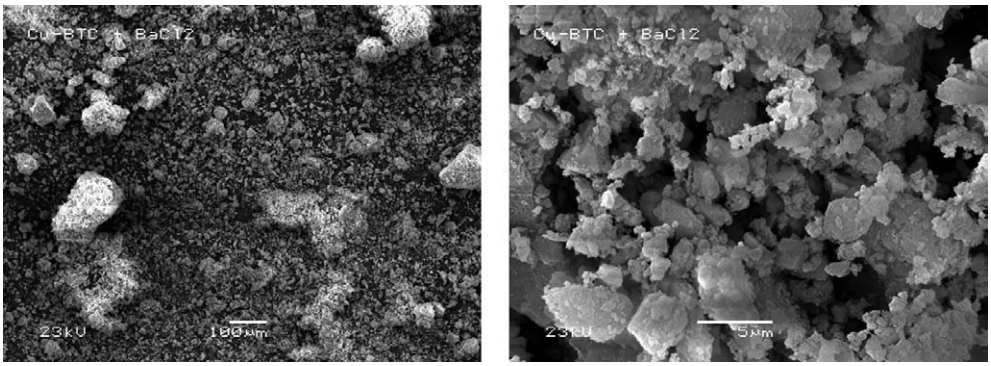

Fig. 5. Scanning electron micrographs of Ba/Cu–BTC(Cl^-).

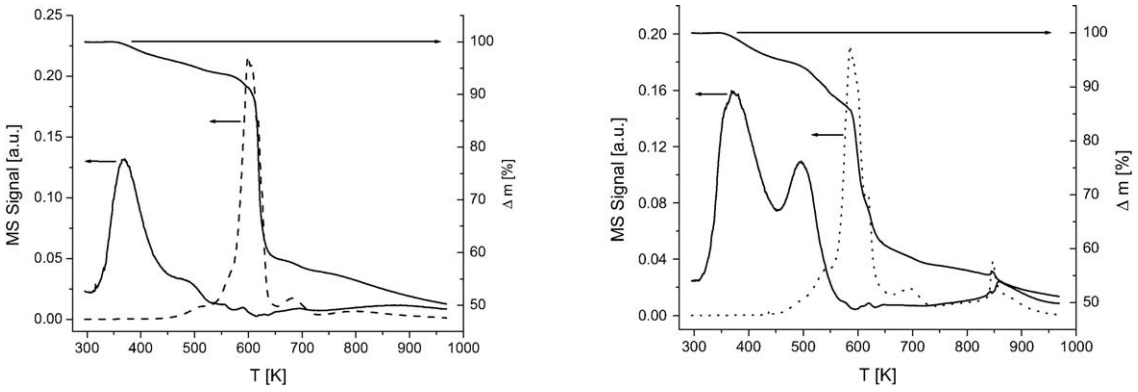

Fig. 6. TGA profiles of Cu–BTC (left) and Ba/Cu–BTC(Cl^-) (right) (295–973 K, full line m/z = 18, dashed line m/z = 44).

EDAX analysis indicated that impregnation with $BaCl_2$ resulted in small Cu–BTC particles covered by barium salt with 5 μm particle size, which agglomerated to bigger particles (~20 μm, Fig. 5). The change in particle morphology compared to the parent Cu–BTC is in good agreement with the general decrease of the intensity of the XRD pattern of this sample.

The changes in sample mass and the evolution of H_2O and CO_2 during temperature increase from 273 and 973 K of Cu–BTC and Ba/Cu–BTC(Cl^-) are compared in Fig. 6. For Cu–BTC, desorption of water (m/z = 18) was observed in the temperature range 323–523 K with two maxima at 373 and 483 K. The mass loss due to the desorption of water was 6.0 wt.%, which according

to the 3 mol water present in the Cu–BTC. The release of CO_2 ($m/z = 44$) indicated that the decarboxylation of the organic linker started at 593 K. The decomposition of the organic linker led to a mass decrease of 44 wt.%, which is in line with the loss of the CO_2 groups from benzene-1,3,5-tricarboxylate. The benzene rings seem to be retained in the sample. For the $BaCl_2$ impregnated Cu–BTC sample the release of H_2O was more pronounced at the maximum around 488 K (weight decrease 10 wt.%), which is attributed to the removal of H_2O retained in higher concentrations by $BaCl_2$. The simultaneous appearance of the maximum for the CO_2 release and for the decrease in the weight indicates that the thermal stability of the Ba-impregnated samples was not affected by the impregnation, i.e. that decarboxylation occurred at the same temperature than with the parent sample.

3.2. State of copper cations

The XANES and the first derivative of the Cu–K edge region of different copper containing references are shown in Fig. 7. The oxidation state of copper can be determined from the position of the absorption edge (see Fig. 7), with a shift to higher energies indicating increasing oxidation state [30–32]. For Cu^+ (8980 eV) and Cu^{2+} species (square-planar symmetry, 8984 eV) the edge positions differ by approx. 4 eV and Cu^{2+} exhibits a further feature at 8976 eV. The edge position and the appearance of specific transitions allow the differentiation between chemical state and the local symmetry of the copper species for each compound [22–25]. The absorption edge results from the dipole-allowed 1s → 4p transition. While Cu^0 and Cu^+ do not have a gap in the 3d orbital, Cu^{2+} compounds are in a d^9 configuration, thus showing a weak, but characteristic pre-edge peak at 8976–8979 eV (quadrupole-allowed 1s → 3d transition with a shoulder at 8986–8989 eV due to the 1s → 4p transition). The 8984 eV (post-edge) feature of Cu^+ complexes has been assigned empirically to a dipole-allowed Cu 1s → 4s transition [26–29]. Cu^{2+} species (e.g. CuO) exhibit a weak pre-edge peak around 8985 eV, which results from the dipole-forbidden 1s → 3d transition. Cu^+ compounds (e.g. Cu_2O and CuCl) show an intense peak at 8980 eV, which is attributed to the dipole-allowed 1s → 4p transition.

XANES and the first derivative of the Cu–K edge region for Cu–BTC and Ba salt impregnated Cu–BTC are shown in Fig. 8. For Cu–BTC and the series of Ba^{2+} impregnated samples an edge position of 8980 eV (main maximum in the first derivative) was observed, which is characteristic for Cu^+. Additionally, for all compounds a second maximum in the derivative spectrum was observed at 8993 eV as well as a shoulder at 8985 eV. These features are assigned in all samples to Cu^{2+} in a square-planar symmetry. The differences in the area under the peaks at 8980 and 8993 eV in the first derivative of the XANES between the Ba/Cu–BTC(Cl^-) and the other samples indicate a higher frac-

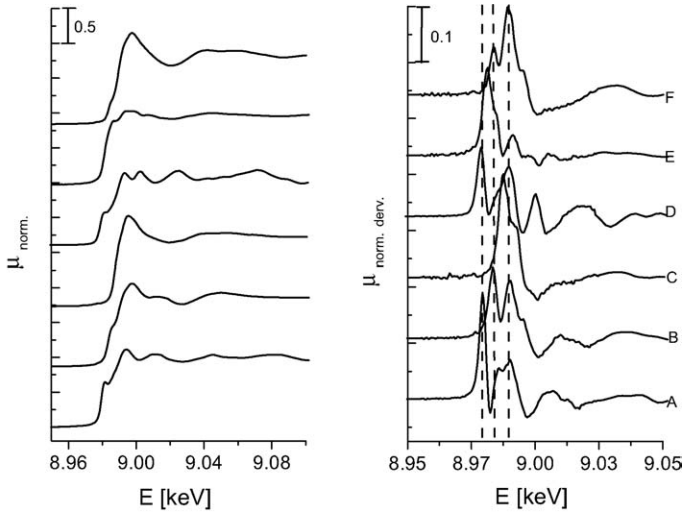

Fig. 7. Cu–K edge XANES of reference materials and their first derivatives; (A) Cu_2O, (B) CuO, (C) $CuSO_4$, (D) Cu, (E) CuCl, (F) $Cu(CH_3COO)_2$).

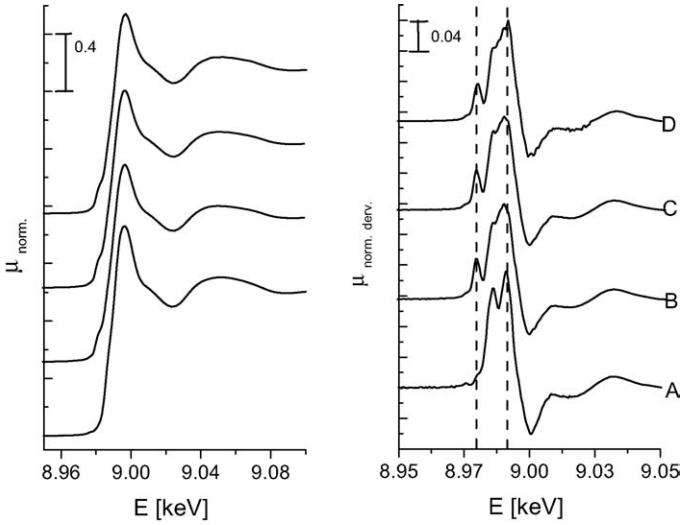

Fig. 8. Cu–K edge XANES of the Ba/Cu–BTC samples and their first derivatives; (A) Cu–BTC with $BaCl_2$ (B) Cu–BTC with $Ba(CH_3COO)_2$, (C) Cu–BTC with $Ba(NO_3)_2$, (D) Parent material.

tion of Cu^{2+} (in square-plane coordination) to be present in the $BaCl_2$ containing sample.

The radial distribution functions (obtained from the Fourier transform of the EXAFS oscillations) of Cu–BTC and Ba/Cu–BTC(Cl^-) are compared to those of CuO and Cu_2O in Fig. 9. The structural properties (obtained by the FEFF fitting) are summarized in Table 2. Both Cu–BTC samples showed one Cu–O contribution with the distance for r_{Cu-O} = 1.91 and 1.94 Å for Cu–BTC and Ba/Cu–BTC(Cl^-), respectively. As synthesis has led to a nearly 100% yield based on the material balance, we conclude that the Cu–O distance in the carboxylates is identical with the distance in CuO. The distance between Cu–Cu in both samples was 2.67 Å, with 0.97 Cu neighbors, in the Cu–BTC and 0.6 in the Ba/Cu–BTC(Cl^-), respectively. The presence of one Cu neighbor in the Cu–BTC sample is in line with the structure of the Cu–BTC structure. Therefore, we conclude that the average number of Cu–Cu neighbors in the sample impregnated with barium chloride indicates a partial destruction of the Cu–BTC structure. Thus, the characterization data indicate that impregnation with $BaCl_2$ affects the local structure of a large fraction of the Cu cations in the metal organic framework.

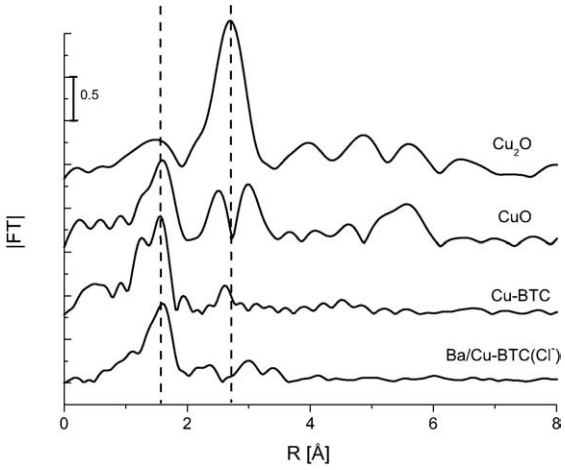

Fig. 9. Fourier Transform of the EXAFS for Ba/Cu–BTC and reference samples (Cu–K edge).

3.3. Storage capacity for SO_2

The SO_2 uptake capacities of the parent Cu–BTC material and the Ba-salt impregnated derivatives were explored between 473 and 773 K and are compared to a conventional $BaCO_3/Al_2O_3$/Pt based material (see Fig. 10).

Table 2
Results from EXAFS analysis from the synthesized MOF samples (S_0^2 = 0.7)

Sample	Atoms	N	R (Å)	σ^2 (Å^2)	E_0 shift (eV)
Cu–BTC	Cu–O	4.05	1.91	0.00720	–7.26
	Cu–Cu	0.97	2.67	0.01200	9.65
Ba/Cu–BTC(Cl^-)	Cu–O	4.21	1.94	0.00748	–8.01
	Cu–Cu	0.60	2.67	0.00958	–4.02

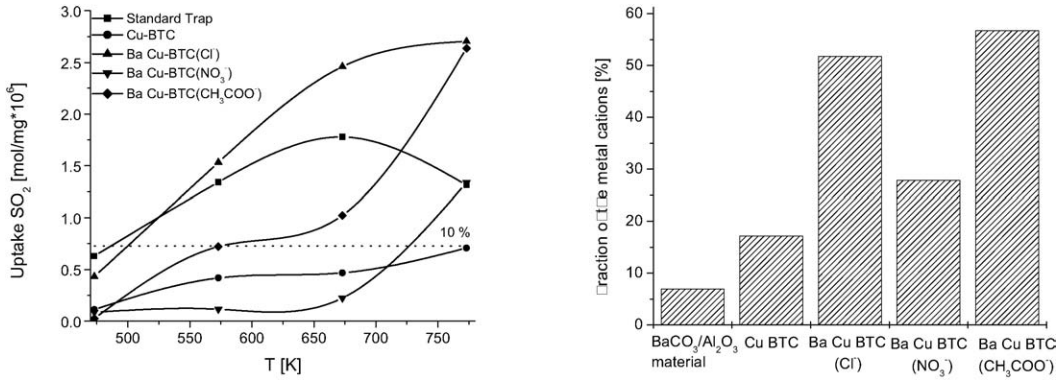

Fig. 10. Uptake capacity (left) and the fraction (right) of the prepared samples.

For Cu–BTC the SO_2 uptake capacity increased with increasing the temperature from 473 to 573 K. A further increase up to 673 K induced only a minor SO_2 uptake. In total, a final storage capacity of 0.7×10^6 mol SO_2 per mg are observed was reached between 473 and 773 K.

The materials impregnated with barium chloride and acetate showed an increasing uptake capacity during heating from 473 up to 573 K, while the nitrate impregnated sample did not show a variation in the capacity compared to the parent material. By heating the samples up to 673 K the uptake capacity for all samples increased. The most marked increase was observed for Cu–BTC impregnated with $BaCl_2$. From 673 to 773 K the uptake increased further, with the strongest being found for the samples impregnated with barium nitrate and acetate. After this procedure the total SO_2 storage capacity of the different impregnated metal organic framework materials were similar for the samples impregnated with barium chloride and acetate, while for the nitrate impregnated sample only half of the capacity was observed.

Also the $BaCO_3/Al_2O_3$/Pt based material (as first generation storage reduction catalyst known to store SO_3) showed an increasing of the uptake capacity during by heating up to 573 and 673 K, respectively. At further increasing temperatures (up to 773 K) desorption of SO_2 was observed leading to the decrease of the SO_2 storage capacity.

At 473 K, $BaCO_3/Al_2O_3$/Pt based material showed the highest uptake, followed by the metal organic framework material impregnated with $BaCl_2$. As the temperature increased to 573 and 673 K the storage capacity increased for all samples, even though only slightly for the Cu–BTC and the nitrate impregnated sample. In the final increase to 773 K the storage capacity for the $BaCO_3/Al_2O_3$/Pt based material decreased, while it increased for all MOF materials. Overall, the highest storage capacities over the entire temperature range were observed for the MOF materials impregnated with barium chloride and barium acetate.

The fractions of metal cations contributing to the chemically binding of SO_2 in the presence of oxygen are compiled in Fig. 10 (right). The amount SO_2 necessary for converting all metal cations into sulfates is defined as 100%. The analysis of the concentrations of SO_2 bound and the concentration of Ba^{2+} and Cu^{+}/Cu^{2+} of the Ba/Cu–BTC samples shows that a significant fraction of the chelated Cu cations are converted into copper sulfates. Similarly, barium and aluminum sulfates are formed upon exposure of $BaCO_3/Al_2O_3$/Pt based material to $SO_2 + O_2$. The results suggest that the cations in the metal organic framework are better utilized than those of the $BaCO_3/Al_2O_3$/Pt based material.

The formation of the various sulfates has profound implications on the thermal stability of the loaded materials as Cu- and Al-sulfates are of lower thermal stability than $BaSO_4$. This variation in stability explains the decreased SO_x storage capacity of the $BaCO_3/Al_2O_3$/Pt based material when the temperature was increased from 673 to 773 K. In this temperature interval (surface) $Al_2(SO_4)_3$ is beginning to be instable and is decomposed to Al_2O_3 and SO_3. It is shown in Table 3 that the impregnation of the metal organic framework materials with Ba-salts leads to a higher SO_x storage capacity. The inclusion of the salt leads to the partial local destruction of the metal organic structure varying

Table 3
SO_2 uptake capacities of the prepared materials in (mol/mg × 10^{-6})

Sample	Uptake (mol/mg × 10^{-6})			
	473 K	573 K	673 K	773 K
$BaCO_3/Al_2O_3$/Pt	0.631	1.341	1.779	1.314
Cu–BTC	0.112	0.418	0.467	0.707
Ba/Cu–BTC(CH_3COO^-)	0.431	1.532	2.460	2.705
Ba/Cu–BTC(NO_3^-)	0.085	0.115	0.223	1.338
Ba/Cu–BTC(Cl^-)	0.026	0.721	1.023	2.637

in extent with the anion used. Higher local destruction by salt impregnation is associated with higher uptake capacity at low temperature. The strongly increased SO_x uptake capacity above 673 K is attributed to the gradual thermal degradation of the lattice and the resulting availability of Cu cations. XRD reveals that $CuSO_4$ and $BaSO_4$ species are formed increasing the concentration with storage temperature.

4. Conclusions

Barium loaded materials impregnated with a metal function for SO_2 oxidations are excellent sorbents for SO_2 in oxygen rich atmosphere. The storage capacity of metal organic framework materials with Cu^+ as central cation and benzene-1,3,5-tricarboxylate (BTC) as linker subsequently impregnated with Ba using $BaCl_2$, $Ba(CH_3COO)_2$ and $Ba(NO_3)_2$ was competitive or better compared to the $BaCO_3/Al_2O_3$/Pt based material. The deposition of the Ba salts leads to small microcrystals of $Ba(CH_3COO)_2$ and $Ba(NO_3)_2$ in pores of the fully intact Cu–BTC together with a decrease in the pore volume. After impregnation of Cu–BTC with $BaCl_2$ the crystallinity of the metal organic framework decreases and Ba-chloride is highly dispersed in the material, therefore, the high pore volume and the well defined structures of the Cu–BTC material offer as well defined and accessible support material.

The Cu–BTC decomposed around 573 K, leading to a complete loss of the Cu–BTC structure. XANES indicates that for the Ba-chloride impregnated sample a significant fraction of copper was oxidized to Cu^{2+}. The other samples did not have a marked concentration of Cu^{2+} (i.e. similar to the parent Cu–BTC). Thus, we conclude that the dispersion of the Ba^{2+} species is the highest in the Ba/Cu–BTC(Cl^-) sample, that the local structure is destroyed for a significant portion of that material and that the accessibility of the Cu cations is drastically enhanced compared to other Ba/Cu–BTC samples. This reveal that the Cu–BTC framework act as a perfect support for the combination between highly dispersed barium (via impregnation with barium chloride) and a highly dispersed form of a oxidation component (partial destroyed metal organic framework).

The highest SO_2 uptake at lower temperatures (<673 K) was observed for Ba/Cu–BTC(Cl^-), while at 773 K the uptake of the Ba/Cu–BTC(Cl^-) and Ba/Cu–BTC(CH_3COO^-) samples (both with the same Ba loading) were identical. The SO_2 uptake of all Ba/Cu–BTC samples exceeded the stoichiometric uptake capacity based on the Ba^{2+} concentration. It is concluded that a fraction of the SO_x is bound to Cu cations. Therefore, the high storage capacity of the Ba/Cu–BTC(Cl^-) material observed not only resulted from the high dispersion of the Ba species, but was also caused by the better accessibility of the Cu cations. At low temperatures the SO_x storage can be described as a physisorption process of SO_2 on Cu cations and the formation of Ba-sulfates, as Cu is still integrated into the metal organic framework. At higher temperatures the metal organic framework is thermally decomposed, which leads to the formation of isolated Cu species that act as SO_x storage sites forming Cu-sulfates. Cu–BTC is a good host material, which provides at low temperature a excellent support properties for the formation of highly dispersed barium, while at higher temperatures, additional storage sites due to the decomposition of the metal organic framework could be formed.

The work presented clearly indicates that impregnated metal organic framework materials are novel suitable components for irreversible SO_x storage, which can be incorporated into advanced non regenerable SO_x traps to enhance the SO_2 storage capacity especially in the low temperature region.

Acknowledgements

Funding from the European Union in the framework of project G3RD-CT2002 00793 is gratefully acknowledged. The authors are also grateful to M. Neukamm for the AAS measurements, X. Hecht for the BET measurements and the staff of the beamline X1 and E4 at Hasylab DESY, Hamburg, Germany for their kind help and continuous support during the experiments.

References

[1] H.K. Chae, D.Y. Siberio-Perez, J. Kim, Y. Go, M. Eddaoudi, A.J. Matzger, M. O'Keefe, O.M. Yaghi, Nature 427 (2004) 523.

[2] H.L. Li, C.E. Davis, T.L. Groy, D.G. Kelley, O.M. Yaghi, J. Am. Chem. Soc. 120 (1998) 2186.

[3] M. Eddaoudi, J. Kim, N. Rosi, D. Vodak, J. Wachter, M. O'Keefe, O.M. Yaghi, Science 295 (2002) 469.

[4] S.R. Batten, Curr. Opin. Solid-State Mat. Sci. 5 (2001) 107.

[5] G. Ferey, Chem. Mater. 13 (2001) 3084.

[6] C.N.R. Rao, S. Natarajan, R. Vaidhyanathan, Angew. Chem. Int. Ed. Engl. 43 (2004) 1466.

[7] H. Li, M. Eddaoudi, T.L. Groy, O.M. Yaghi, J. Am. Chem. Soc. 120 (1998) 8571.

[8] S.S.Y. Chui, S.M.F. Lo, J.P.H. Charmant, A.G. Orpen, I.D. Williams, Science 283 (1999) 1148.

[9] H. Li, M. Eddaoudi, M. O'Keeffe, O.M. Yaghi, Nature 402 (1999) 276.

[10] B.L. Chen, M. Eddaoudi, S.T. Hyde, M. O'Keeffe, O.M. Yaghi, Science 291 (2001) 1021.

[11] M. Eddaoudi, H.L. Li, O.M. Yaghi, J. Am. Chem. Soc. 122 (2000) 1391.

[12] A. Vishnyakov, P.I. Ravikovitch, A.V. Neimark, M. Bulow, Q.M. Wang, Nano Lett. 3 (2003) 713.

[13] O.M. Yaghi, C.E. Davis, G.M. Li, H.L. Li, J. Am. Chem. Soc. 119 (1997) 2861.

[14] N.L. Rosi, J. Eckert, M. Eddaoudi, D.T. Vodak, J. Kim, M. O'Keeffe, O.M. Yaghi, Science 300 (2003) 1127.

[15] M. Eddaoudi, D.B. Moler, H.L. Li, B.L. Chen, T.M. Reineke, M. O'Keeffe, O.M. Yaghi, Acc. Chem. Res. 34 (2001) 319.

[16] Q.M. Wang, D. Shen, M. Bulow, M.L. Lau, F.R. Fitch, S.G. Deng, US Patent 6,491,740, 2002.

[17] Q.M. Wang, D.M. Shen, M. Bulow, M.L. Lau, S.G. Deng, F.R. Fitch, N.O. Lemcaff, J. Semanscin, Microporous Mesoporous Mat. 55 (2002) 217.

[18] A. Amberntsson, M. Skoglundh, M. Jonsson, E. Fridell, Catal. Today 73 (2002) 279.

[19] A. Amberntsson, M. Skoglundh, S. Ljungstrom, E. Fridell, J. Catal. 217 (2003) 253.

[20] K.V. Klementev, J. Phys. D Appl. Phys. 34 (2001) 209.

[21] A.L. Ankudinov, J.J. Rehr, Phys. Rev. B 62 (2000) 2437.

[22] W.B. Kim, J.S. Lee, J. Phys. Chem. B 107 (2003) 9195.

[23] C. Prestipino, S. Bordiga, C. Lamberti, S. Vidotto, M. Garilli, B. Cremaschi, A. Marsella, G. Leafanti, P. Fisicaro, G. Spoto, A. Zecchina, J. Phys. Chem. B 107 (2003) 5022.

[24] L.S. Kau, D.J. Spirasolomon, J.E. Pennerhahn, K.O. Hodgson, E.I. Solomon, J. Am. Chem. Soc. 109 (1987) 6433.

[25] F. Xamena, P. Fisicaro, G. Berlier, A. Zecchina, G.T. Palomino, C. Prestipino, S. Bordiga, E. Giamello, C. Lamberti, J. Phys. Chem. B 107 (2003) 7036.

[26] V.W. Hu, S.I. Chan, G.S. Brown, Proc. Natl Acad. Sci. USA 74 (1977) 3821.

[27] L. Powers, W.E. Blumberg, B. Chance, C. Barlow, J.S. Leight Jr., J.C. Smith, T. Yonetani, S. Vik, J. Peisach, J. Biochim. Biophys. Acta 546 (1979) 520.

[28] W.E. Blumberg, J. Peisach, P. Eisenberger, J.A. Fee, Biochemistry 17 (1978) 1842.

[29] J.M. Brown, L. Powers, B. Kincaid, J.A. Larrabee, T.G. Spiro, J. Am. Chem. Soc. 102 (1980) 4210.

[30] Y.J. Huang, H.P. Wang, J. Phys. Chem. A 103 (1999) 6514.

[31] Y.J. Huang, H.P. Wang, J.F. Lee, Appl. Catal. B-Environ. 40 (2003) 111.

[32] C. Lamberti, S. Bordiga, F. Bonino, C. Prestipino, G. Berlier, L. Capello, F. D'Acapito, F. Xamena, A. Zecchina, Phys. Chem. Chem. Phys. 5 (2003) 4502.